Repair of injured plasma membrane by rapid Ca^{2+}-dependent endocytosis

Vincent Idone,[1] Christina Tam,[1] John W. Goss,[2] Derek Toomre,[2] Marc Pypaert,[2] and Norma W. Andrews[1,2]

[1]Section of Microbial Pathogenesis and [2]Department of Cell Biology, Yale University School of Medicine, New Haven, CT 06510

Ca^{2+} influx through plasma membrane lesions triggers a rapid repair process that was previously shown to require the exocytosis of lysosomal organelles (Reddy, A., E. Caler, and N. Andrews. 2001. *Cell.* 106:157–169). However, how exocytosis leads to membrane resealing has remained obscure, particularly for stable lesions caused by pore-forming proteins. In this study, we show that Ca^{2+}-dependent resealing after permeabilization with the bacterial toxin streptolysin O (SLO) requires endocytosis via a novel pathway that removes SLO-containing pores from the plasma membrane. We also find that endocytosis is similarly required to repair lesions formed in mechanically wounded cells. Inhibition of lesion endocytosis (by sterol depletion) inhibits repair, whereas enhancement of endocytosis through disruption of the actin cytoskeleton facilitates resealing. Thus, endocytosis promotes wound resealing by removing lesions from the plasma membrane. These findings provide an important new insight into how cells protect themselves not only from mechanical injury but also from microbial toxins and pore-forming proteins produced by the immune system.

Introduction

When the plasma membrane of eukaryotic cells is mechanically injured, Ca^{2+} influx triggers a rapid repair process that involves exocytosis (Reddy et al., 2001; McNeil, 2002; McNeil et al., 2003). Although the precise repair mechanism is still unknown, current hypotheses propose that resealing is directly mediated by the delivery of intracellular membrane to the cell surface. These models suggest that Ca^{2+}-dependent exocytosis acts by providing a membrane patch (McNeil et al., 2000) or by relieving plasma membrane tension, which facilitates resealing (Togo et al., 2000). However, such models cannot explain the process by which cells repair the stable protein-lined transmembrane lesions caused by pore-forming proteins (Campbell and Morgan, 1985; Browne et al., 1999; Walev et al., 2001; Keefe et al., 2005).

Experiments using the complement membrane attack complex (Morgan and Campbell, 1985) or the bacterial toxin streptolysin O (SLO; Walev et al., 2001) found that membrane resealing after pore formation is also Ca^{2+} dependent. Despite this common requirement, until now, the repair of transmembrane pores was largely viewed as a process distinct from the resealing of mechanical wounds and was assumed to involve considerably longer periods of time. In this study, we show that SLO-permeabilized cells reseal with the same fast kinetics previously reported for the repair of mechanical wounds (Steinhardt et al., 1994; Reddy et al., 2001) and demonstrate that both processes involve a rapid form of Ca^{2+}-dependent endocytosis.

Correspondence to Norma W. Andrews: norma.andrews@yale.edu

Abbreviations used in this paper: MβCD, methyl–β-cyclodextrin; NRK, normal rat kidney; PI, propidium iodide; SLO, streptolysin O; TR, Texas red; WGA, wheat germ agglutinin.

The online version of this article contains supplemental material.

Results and discussion

Our initial observations showed that SLO-permeabilized cells reseal significantly faster than previously reported (Walev et al., 2001). In the presence of Ca^{2+}, normal rat kidney (NRK) cells exposed to SLO excluded the membrane-impermeant dye propidium iodide (PI) after 4 min (Fig. 1 A). Cells permeabilized without Ca^{2+} only resealed after Ca^{2+} addition (Fig. S1 A, available at http://www.jcb.org/cgi/content/full/jcb.200708010/DC1), and pores formed at high SLO concentrations were less efficiently repaired (Fig. 1 A). Resealing was similar in NRK (rat), HEK-293, and HeLa (human) cells and was inhibited after ATP depletion (Fig. 1 B).

To determine the precise kinetics of SLO pore repair, time-lapse video microscopy was performed in cells loaded with the Ca^{2+}-sensitive dye Fluo-3. Upon SLO permeabilization, cells showed transient increases in intracellular fluorescence, reflecting an influx of Ca^{2+} followed by resealing (Video 1, available at http://www.jcb.org/cgi/content/full/jcb.200708010/DC1). Under normal conditions, $[Ca^{2+}]_i$ returned to baseline in ~30 s, whereas it remained elevated in cells pretreated with ATP-depleting agents (Fig. 1 C). The fast kinetics of SLO pore repair was confirmed by imaging cells stained with the lipophilic dye

The Journal of Cell Biology, Vol. 180, No. 5, March 10, 2008 905–914
http://www.jcb.org/cgi/doi/10.1083/jcb.200708010

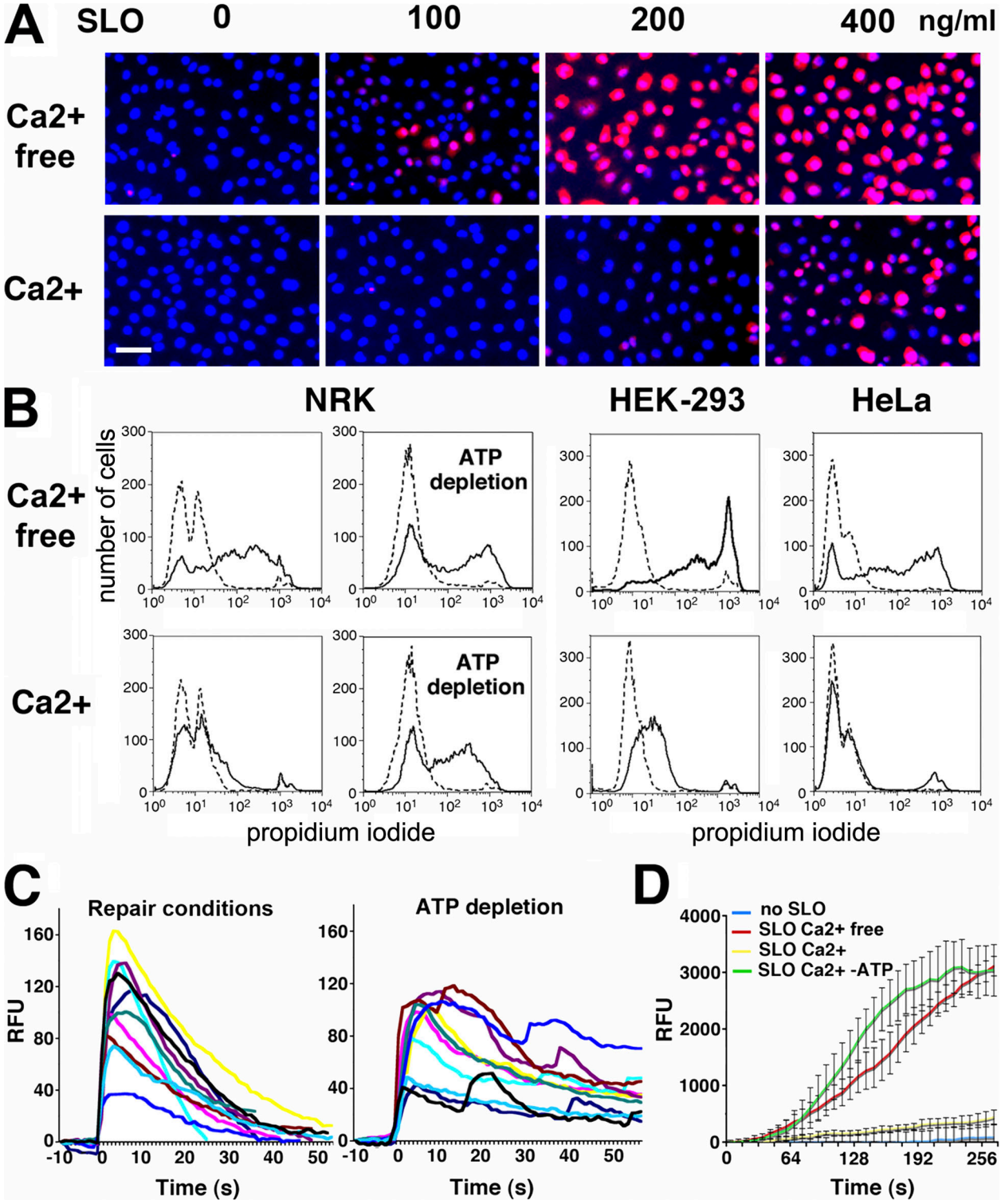

Figure 1. **Plasma membrane resealing after SLO permeabilization is rapid and requires Ca^{2+} and ATP.** (A) Resealing of SLO-permeabilized NRK cells is Ca^{2+} dependent and decreases as toxin concentrations increase. DAPI staining (blue) shows all nuclei; PI staining (red) shows cells that failed to reseal. Bar, 10 µm. (B) FACS of PI staining showing Ca^{2+}- and ATP-dependent resealing of cells permeabilized with 200 ng/ml SLO. Dashed lines, no SLO; solid lines, SLO. (C) Ca^{2+} influx into NRK cells loaded with Fluo-3 and exposed to 175 ng/ml SLO stops rapidly under repair conditions but is sustained in ATP-depleted cells. $[Ca^{2+}]_i$ transient traces were aligned for graphical representation. See Video 1. (D) FM1-43 influx into HEK-293 cells permeabilized with 200 ng/ml SLO stops rapidly in the presence of Ca^{2+} but is sustained in the absence of Ca^{2+} or ATP. The data represent the mean ± SD (error bars) of intracellular fluorescence intensity in five cells. See Video 2 (available at http://www.jcb.org/cgi/content/full/jcb.200708010/DC1). RFU, relative fluorescence units.

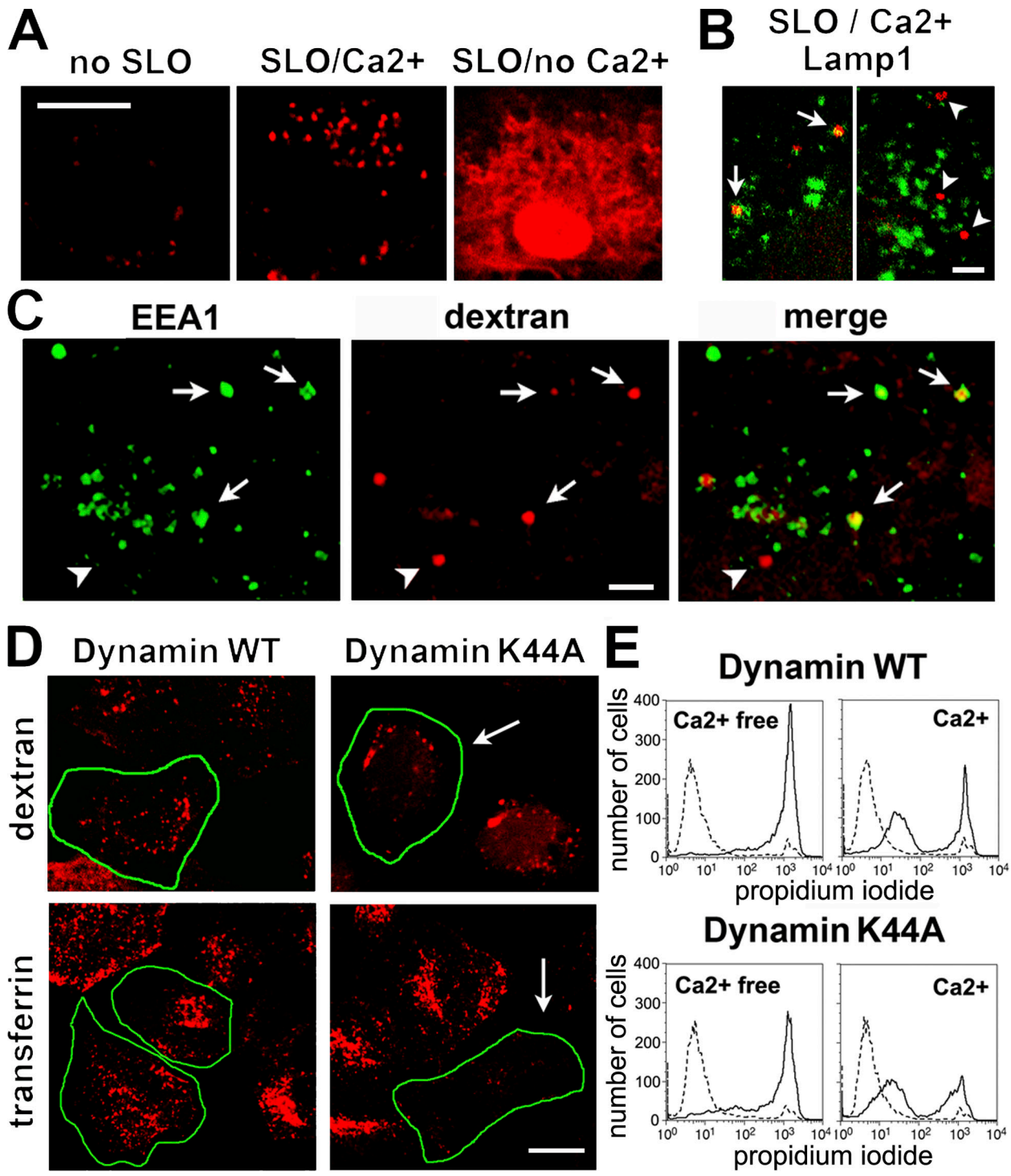

Figure 2. **Cells permeabilized by SLO in the presence of Ca^{2+} undergo dynamin-2–independent endocytosis.** (A) NRK cells exposed or not exposed to 250 ng/ml SLO were incubated for 4 min with TR dextran. In SLO/Ca^{2+}, dextran is detected in multiple intracellular vesicles; without Ca^{2+}, it enters the cytosol through SLO pores. (B) Dextran-containing vesicles (red) colocalize partially (arrows) or do not colocalize (arrowheads) with mAbs to Lamp-1 (LY1C6; green). Two independent confocal z sections are shown. (C) Most dextran-containing endosomes (red) colocalize with antibodies to EEA1 (green). Arrows indicate vesicles colocalizing with antibodies; arrowheads indicate one vesicle not colocalizing. (D) NRK cells expressing dynamin-2–GFP internalize transferrin (red; bottom left) or TR dextran after SLO/Ca^{2+} (red; top left). Cells expressing K44A dynamin-2–GFP exclude transferrin (bottom right; arrow) but still endocytose dextran after SLO/Ca^{2+} (top right; arrow). Transfected cells are outlined in green. WT, wild type. (E) FACS of PI staining (gated on GFP^+ cells) shows that Ca^{2+}-dependent resealing of SLO-permeabilized NRK cells is not inhibited by K44A dynamin-2–GFP. Dashed lines, no SLO; solid lines, SLO. Bars: (A and D) 5 µm; (B and C) 1 µm.

FM1-43. In intact cells, FM1-43 remains in the plasma membrane, but when bilayer integrity is breached, it rapidly partitions into intracellular membranes. Cells exposed to SLO in the presence of Ca^{2+} showed only a slight increase in intracellular staining. In contrast, FM1-43 rapidly flowed into cells in the absence of Ca^{2+} or after ATP depletion. When Ca^{2+} was present,

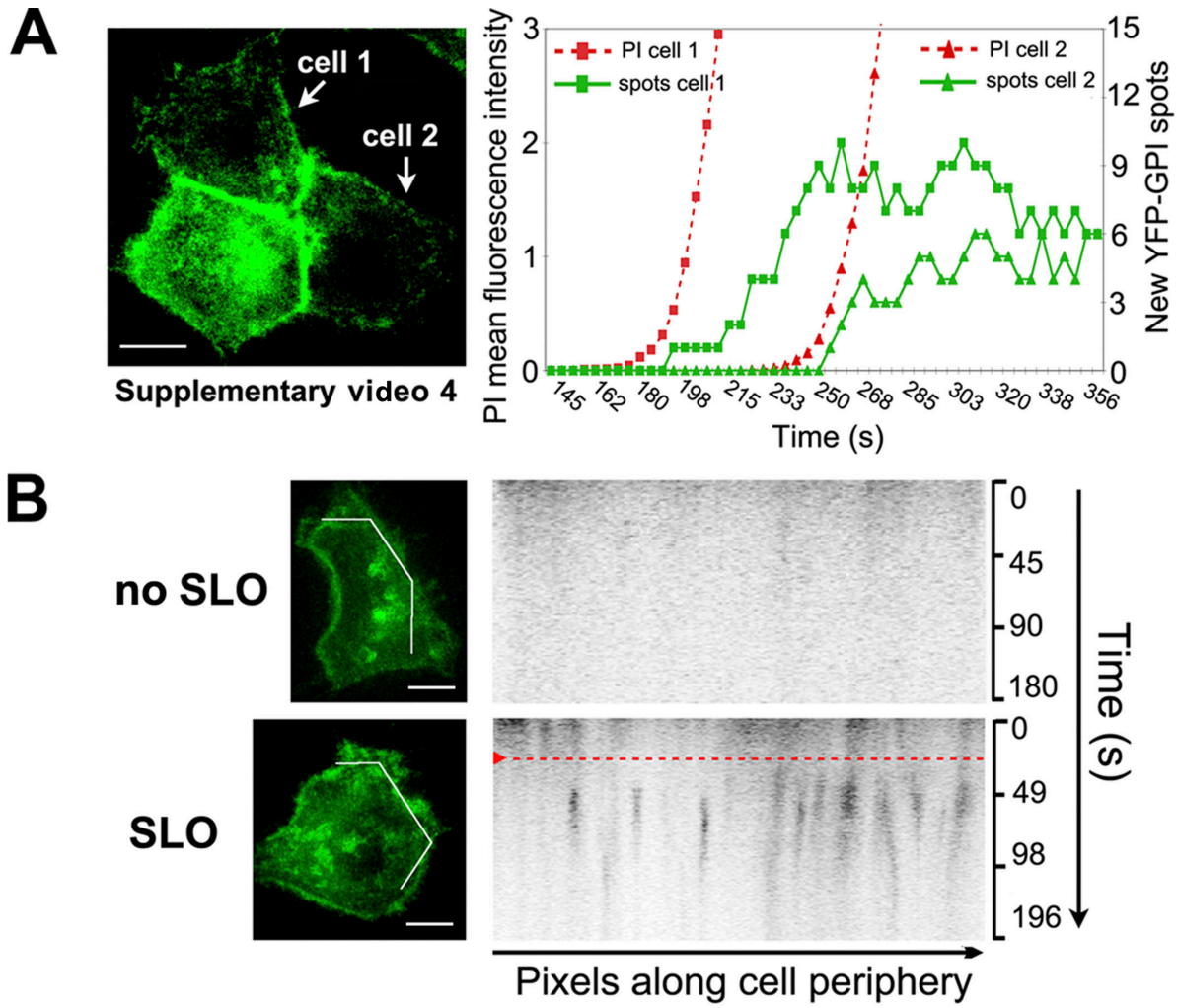

Figure 3. **SLO pores trigger rapid endocytosis in the presence of Ca^{2+}.** (A–C) Live confocal imaging showing rapid endocytosis in HeLa cells expressing YFP-GPI (green) on the plasma membrane. (A) After exposure to 250 ng/ml SLO and PI (red), the two cells analyzed initiated endocytosis 5–15 s after

FM1-43 influx was blocked in <30 s, confirming that SLO-permeabilized cells reseal within this period (Fig. 1 D and Video 2). Thus, transmembrane pores can be repaired with the same rapid kinetics previously observed for the resealing of mechanical wounds (Steinhardt et al., 1994; Reddy et al., 2001).

SLO pore formation is strictly dependent on plasma membrane cholesterol. The process is initiated by the binding of toxin monomers to the plasma membrane followed by oligomerization and a conformational change that drives membrane insertion, resulting in a pore of ~30 nm in diameter (Tweten, 2005). Resealing requires removal or disassembly of the transmembrane pores. Disassembly is unlikely to be responsible for restoring plasma membrane integrity because pore resealing is rapid and strongly dependent on target cell ATP. Studies of cells permeabilized by complement suggested that pore removal might occur by two possible mechanisms: (1) release in the form of plasma membrane blebs (Morgan, 1989) and/or (2) internalization (Carney et al., 1985; Morgan et al., 1987). Investigating the first possibility, we imaged cells stained with FM1-43 during SLO exposure. In the presence of Ca^{2+}, prominent plasma membrane blebs formed in HEK-293 (Video 2 and Fig. S2, available at http://www.jcb.org/cgi/content/full/jcb.200708010/DC1), HeLa, and NRK cells (not depicted). However, instead of being released, the blebs retracted back into the cell body (Fig. S2, A and B; and Video 2). In all cells examined, bleb formation followed by retraction involved >1 min; this is slower than plasma membrane resealing, which occurs in <30 s. Moreover, resealing still occurred after blebbing was blocked with cytochalasin D (Fig. S2 C and Video 3; Charras et al., 2006), showing that blebs are not responsible for pore removal. Blebbing may result from Ca^{2+}-induced disruption in the cortical cytoskeleton, with retraction reflecting recovery of the contractile actin cortex after resealing (Charras et al., 2006).

Next, we investigated whether SLO pores were removed from the plasma membrane by endocytosis. Within 4 min of adding SLO in the presence of Ca^{2+} and a membrane-impermeable fluorescent dextran, numerous endosomes containing the tracer were detected. Without SLO, dextran uptake was only faintly visible after a similar period, which is consistent with the slow constitutive endocytosis rate of these cells. Without Ca^{2+}, SLO-permeabilized cells did not reseal, and the tracer entered the cytosol (Fig. 2 A). The lysosomal marker Lamp1 was detected on a few SLO/Ca^{2+}-induced endosomes (Fig. 2 B), whereas more extensive colocalization was seen with the early endosome marker EEA1 (Fig. 2 C). To determine whether this form of endocytosis was dynamin dependent, we expressed the dominant-negative K44A mutant of dynamin-2 that inhibits endocytosis of clathrin-coated vesicles, caveolae, and some types of lipid raft–dependent vesicles (van der Bliek et al., 1993; Oh et al., 1998; Lamaze et al., 2001). Dynamin-2 K44A strongly reduced transferrin uptake but did not inhibit the formation of SLO/Ca^{2+}-triggered endosomes (Fig. 2 D) or cell resealing (Fig. 2 E).

The endosomes formed in response to SLO/Ca^{2+} were good candidates for removing SLO pores from the plasma membrane. Because membrane repair after SLO pore formation occurs within 10–30 s (Fig. 1, C and D), we investigated whether the kinetics of endocytosis coincided with this period. The plasma membrane of HeLa cells was labeled with a transduced YFP-GPI adenovirus construct (YFP-GL-GPI; Keller et al., 2001), and confocal images were rapidly acquired. Within 5–15 s after SLO permeabilization, numerous vesicles containing YFP-GPI were observed inside the cells. In contrast, there was minimal internalization of YFP-GPI in cells not permeabilized by SLO (Fig. 3, A and B; and Videos 4 and 5, available at http://www.jcb.org/cgi/content/full/jcb.200708010/DC1). To visualize the early dynamics of the toxin in contact with cells, active Cherry-tagged SLO was generated (Fig. S1 B). When locally added to cells, Cherry-SLO permeabilized cells within 12–14 s (assessed by FM1-43 influx; unpublished data). In the absence of Ca^{2+}, a condition that causes full cell permeabilization (Fig. S1 B), the toxin remained associated with the plasma membrane (Fig. 3 C and Video 6). In contrast, when Ca^{2+} was present, plasma membrane–associated Cherry-SLO rapidly partitioned into dynamic peripheral spots, some of which colocalized with recently formed YFP-GPI endosomes (Fig. 3 C and Video 7). Thus, SLO/Ca^{2+} triggers the formation of endosomes containing GPI-anchored molecules and SLO within the few seconds involved in restoration of plasma membrane integrity. Although these observations do not directly demonstrate the presence of functional SLO pores in the endosomes, they are consistent with endocytosis being the mechanism for pore removal.

The number of endocytic vesicles within the cells was significantly increased in the presence of Ca^{2+}. These vesicles were large (mean diameter of 0.3–0.5 µm) and often contained membrane invaginations (Fig. 4 A). Peripheral endosomes of similar size and morphology were detected in cells wounded by scraping (Fig. 4 B). As observed in SLO-permeabilized cells, the absence of Ca^{2+} during wounding resulted in markedly less vesicles containing the endocytic tracer (Fig. 4 B). Ca^{2+}-dependent large endosomes were also observed by EM in cells wounded by electroporation (unpublished data).

Our observation of YFP-GPI partitioning into SLO-induced endosomes (Fig. 3) and the fact that SLO interacts with membrane cholesterol during pore formation (Tweten, 2005) suggested a role for cholesterol-rich membrane domains in this endocytic mechanism. Taking advantage of the fact that Ca^{2+}-dependent endosomes are also induced in scrape-wounded cells, we investigated the effect of acute cholesterol depletion in endocytosis and plasma membrane repair. Dose-dependent inhibition

pore formation (indicated by PI influx). The graph shows quantification of PI fluorescence and newly formed YFP-GPI intracellular spots. See Video 4. (B) Kymographs of YFP-GPI fluorescence along a line drawn across the periphery of cells imaged for 3 min. The red dashed line indicates when 100 µg/ml SLO was locally added. Endosomes (dark pixels) were first detected 5–10 s after SLO addition. See Video 5. (C) HeLa cells expressing YFP-GPI (green) and exposed to Cherry-SLO (red) locally with or without Ca^{2+}. Individual spots containing both YFP-GPI and Cherry-SLO seen moving into the cell are indicated (the arrowheads, short arrows, and long arrows point to each of three examples of these spots). See Videos 6 and 7 (available at http://www.jcb.org/cgi/content/full/jcb.200708010/DC1). Bars: (A and B) 10 µm; (C) 5 µm.

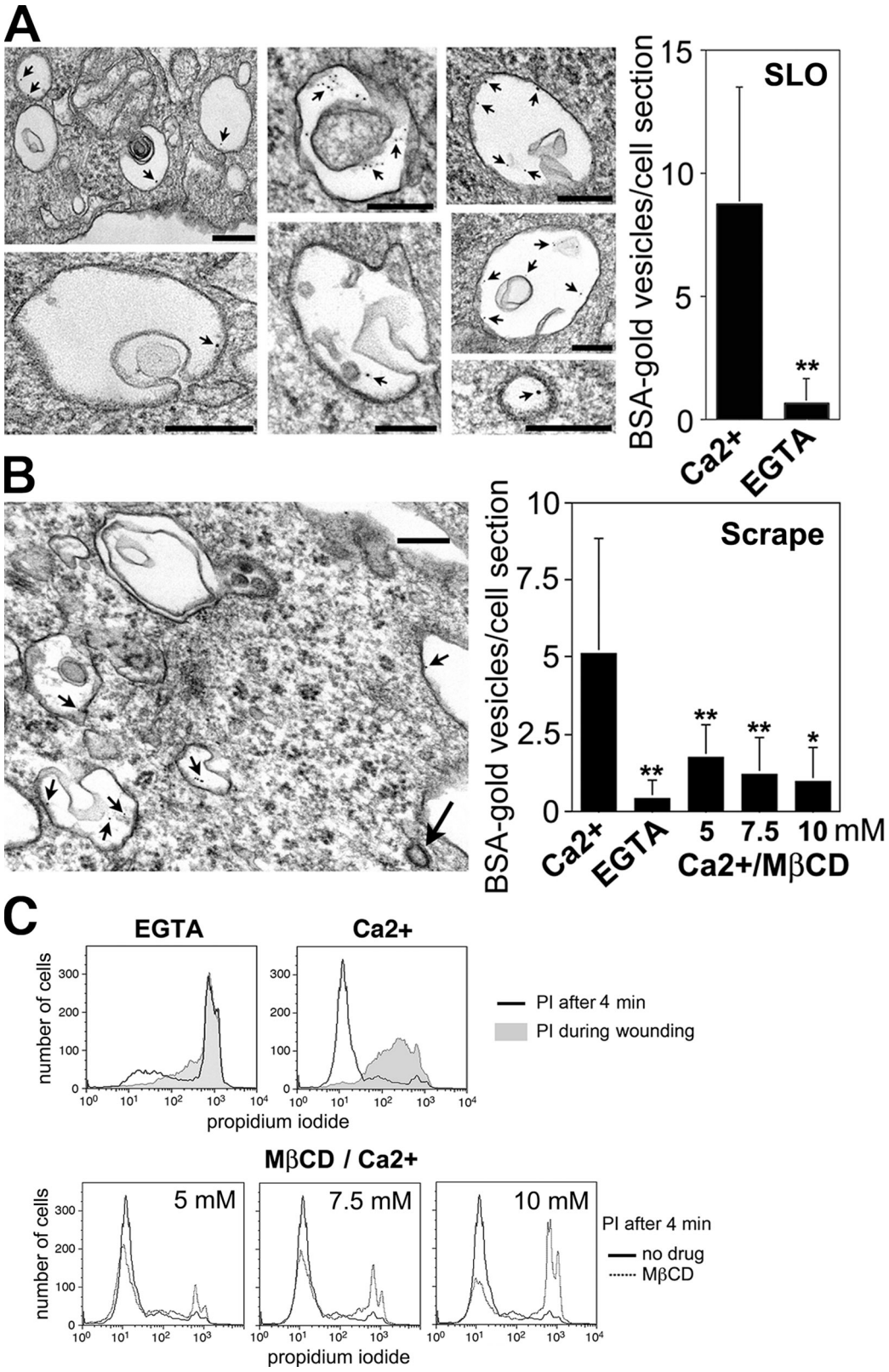

Figure 4. **Large Ca^{2+} and cholesterol-dependent endosomes are induced by plasma membrane injury.** (A) EM showing endosomes formed in NRK cells 4 min after exposure to SLO in the presence of Ca^{2+} and BSA-gold. Arrows point to gold particles. (bottom right) Clathrin-coated vesicle found in the same cells. (right) Quantification shows ~13-fold less BSA-gold–containing vesicles in cells permeabilized by SLO without Ca^{2+}. The data represent the mean ± SD (error bars). **, $P < 0.0001$ (unpaired *t* test). (B) EM showing similar endosomes 4 min after scrape wounding HeLa cells. Short arrows, BSA-gold particles; long arrow, clathrin-coated vesicle. (right) Quantification shows less BSA-gold–containing vesicles in cells scraped without Ca^{2+} or in Ca^{2+} after cholesterol extraction with MβCD. The data represent the mean ± SD (error bars). *, $P < 0.005$; **, $P < 0.0001$ (unpaired *t* test). (C) Cholesterol depletion inhibits wound repair. HeLa cells were treated with MβCD and analyzed by FACS after scrape wounding (gray fill, PI added during wounding). Bars, 200 nm.

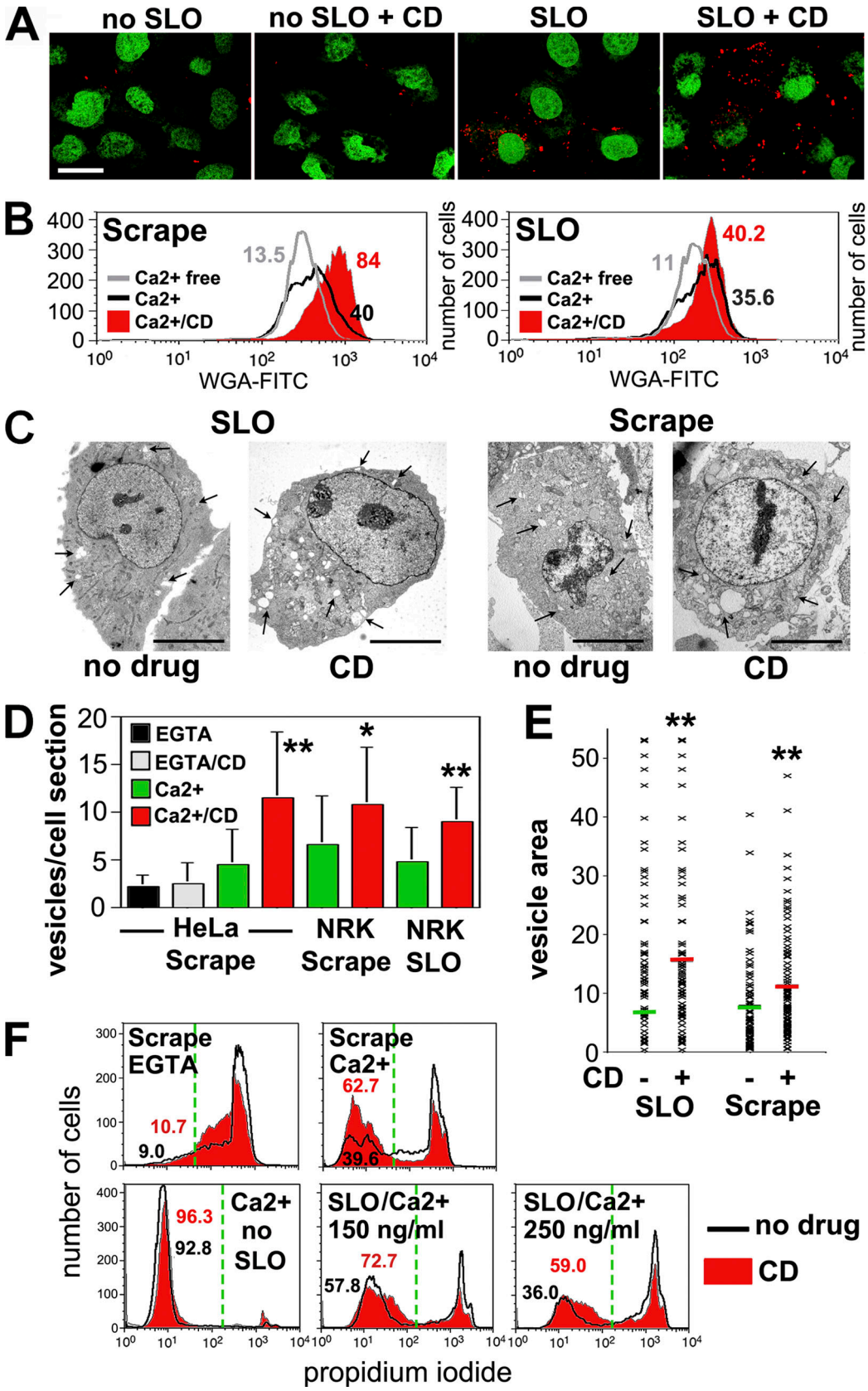

Figure 5. **Disruption of the actin cytoskeleton enhances endocytosis and resealing in cells permeabilized by SLO pores or mechanical wounds.** (A) NRK cells treated or not treated with cytochalasin D (CD) were exposed or not exposed to 250 ng/ml SLO for 4 min in the presence of TR dextran (red). (B) Endocytosis was quantified with a trypan blue quenching FACS assay in HeLa (left) or NRK (right) cells labeled with WGA-FITC and wounded by SLO or by scraping. The percentage of cells with WGA-FITC protected from quenching is indicated, showing that cytochalasin D (red fill) enhances endocytosis. (C) EM of NRK cells treated or not treated with cytochalasin D and fixed 4 min after 200 ng/ml SLO or scraping in Ca^{2+}. The increase in endosome

of endocytosis and plasma membrane resealing was observed after cholesterol extraction with methyl–β-cyclodextrin (MβCD; Fig. 4, B and C), providing a direct link between injury-induced endocytosis and plasma membrane repair.

The rapid endocytosis induced by SLO/Ca^{2+} was enhanced after treatment with drugs that interfere with actin polymerization, cytochalasin D (Fig. 5 A), or latrunculin A (not depicted). Cytochalasin D enhanced Ca^{2+}-dependent endocytosis in cells injured by SLO or scraping, as shown by quantitative quench protection (Fig. 5 B and Fig. S3 A, available at http://www.jcb.org/cgi/content/full/jcb.200708010/DC1) and EM assays (Fig. 5, C and D). Importantly, cytochalasin D treatment also increased the mean size of endosomes (Fig. 5, C and E; and Fig. S3 B) and enhanced resealing in cells injured by both conditions (Fig. 5 F). These results demonstrate a direct correlation between the extent of endocytosis and that of plasma membrane repair.

Consistent with our findings, an earlier study reported the rapid formation of EEA1-positive endosomes in target cells permeabilized by the cytotoxic T lymphocyte pore-forming protein perforin (Keefe et al., 2005). However, because perforin requires Ca^{2+} to form pores, the Ca^{2+} requirement of this endocytic process could not be directly assessed. Ca^{2+} influx induced by ionomycin failed to induce endocytosis, leading Keefe et al. (2005) to conclude that perforin-induced endocytosis was not triggered by Ca^{2+} and, thus, was unrelated to the target cell resealing mechanism. However, it is important to note that Ca^{2+} ionophores cause irreversible cellular damage, including a rapid ATP depletion (Gmitter et al., 1996) that can explain the block in endocytosis. Because SLO forms pores with or without Ca^{2+} (Fig. S1 A), we could directly demonstrate that both endocytosis and plasma membrane repair require extracellular Ca^{2+}. Thus, it is likely that the pore-induced Ca^{2+}-dependent endocytosis we describe here also mediates plasma membrane repair in cells subjected to CTL attack.

Ca^{2+} influx into injured cells triggers lysosomal exocytosis, a response required for efficient plasma membrane resealing (Rodriguez et al., 1997; Reddy et al., 2001; McNeil et al., 2003). Thus, the rapid endocytosis induced by SLO or scraping in the presence of Ca^{2+} may represent a compensatory response to lysosomal exocytosis. Compensatory endocytosis, although mostly studied in specialized neurosecretory cells (Gundelfinger et al., 2003), is detected after exocytosis in several cell types (Ninomiya et al., 1996; Cocucci et al., 2004, 2007).

Collectively, our findings suggest that injury-induced endocytosis represents an important cellular defense mechanism against pore-forming proteins generated endogenously (complement and perforin) or exogenously (bacterial toxins). Moreover, rapid endocytosis also appears to participate in the removal of lesions created by mechanical tears. In future studies, it will be important to determine whether defects in this endocytic pathway occur in genetic syndromes showing deficient plasma membrane repair but normal Ca^{2+}-dependent exocytosis (Jaiswal et al., 2007). Characterization of the molecular machinery involved in generating injury-dependent endosomes should provide powerful new tools for further dissecting the fundamental process of plasma membrane repair.

Materials and methods

Plasma membrane repair assays

Cells were cultured at 37°C in 5% CO_2 in high glucose DME and 10% FBS containing penicillin/streptomycin (Invitrogen). SLO was purified from BL21 *Escherichia coli* expressing 6× histidine-tagged SLO (cloned into pTrcHisA; Invitrogen; plasmid provided by R. Tweeten, University of Oklahoma, Norman, OK). Cherry-SLO plasmid was constructed by inserting mCherry (Shaner et al., 2004) N terminal to SLO in pTrcHisA-SLO. mCherry was amplified by PCR from mCherry-pRSET-B (Shaner et al., 2004) with primers 5′-ACGCGTCGACGGATGGTGAGCAAGGGCGAGG-3′ and 5′-ACGCGTCGACTTGTACAGCTCGTCCATGCCG-3′ to append SalI sites onto each end. After SalI digestion, mCherry was ligated into a unique engineered SalI site in pTrcHisA-SLO at 282–961 bp.

Cell monolayers (60% confluence) were washed at 4°C with Ca^{2+}-free DME containing 5 mM EGTA followed by two more washes in Ca^{2+}-free DME. SLO was bound to target cells in Ca^{2+}-free DME for 5 min at 4°C, and pore formation was triggered by replacing the medium with 37°C DME containing or not containing1.8 mM Ca^{2+}. Experiments performed in buffers containing identical concentrations of free Ca^{2+} or Mg^{2+} (Rodriguez et al., 1997) demonstrated that 1 μM Ca^{2+} (but not 1 μM Mg^{2+}) was sufficient to promote resealing. After 4 min at 37°C, cells were stained for 1 min with 50 μg/ml PI (Sigma-Aldrich), fixed in 4% PFA, and imaged by a microscope (Axiovert 200; Carl Zeiss, Inc.) equipped with a camera (CoolSNAP HQ; Roper Scientific) and MetaMorph software (MDS Analytical Technologies) or by a confocal microscope (LSM500; Carl Zeiss, Inc.). For FACS assays, 2 × 10^6 trypsinized cells were incubated with SLO in suspension for 5 min at 4°C in 250 μl of Ca^{2+}-free DME followed by resuspension in 37°C medium containing or not containing Ca^{2+} and PI staining (4-min total incubation time). In scrape wounding assays, cells were removed from the dish at 37°C with a rubber policeman (Becton Dickinson), and PI was added either during scraping or after 4 min at 37°C in the presence or absence of Ca^{2+} (Ca^{2+}-free medium contained 10 mM EGTA). After flow cytometry (FACSCalibur; Becton Dickinson) of at least 10,000 cells, the data were analyzed using FlowJo v6.3 software (Tree Star, Inc.).

Drug treatments

ATP was depleted by pretreating cells for 1 h with 10 mM sodium azide and 20 mM 2-deoxyglucose (Sigma-Aldrich) in glucose-free DME. Cytochalasin D or latrunculin A (Sigma-Aldrich) was added to the incubation medium at 1 μg/ml for 45 min and maintained at the same concentration during the assays. Cholesterol was extracted by pretreating cells with the indicated concentrations of MβCD in DME, 0.2% BSA, and 10 mM Hepes/NaOH, pH 7, for 45 min.

Live time-lapse imaging

Subconfluent cells plated on glass-bottom dishes (Mattek) were loaded with Fluo-3 (Invitrogen) as described previously (Reddy et al., 2001) or were incubated with 4 μM FM1-43 (Invitrogen) before exposure to SLO in 37°C DME containing or not containing Ca^{2+} (Invitrogen). Dishes were placed on a heated stage (37°C), and time-lapse imaging on an Axiovert 200 microscope equipped with a CoolSNAP HQ camera or an LSM510 confocal microscope was initiated immediately at 1- (Fluo-3) or 6-s (FM1-43) intervals for 5 min. Quantitative analysis of intracellular fluorescence was performed using MetaMorph software. Confocal spinning disk microscopy (PerkinElmer) was performed in cells transduced with adenovirus encoding YFP-GL-GPI (Keller et al., 2001) on a 37°C heated stage as previously

number/size (clear vesicles; arrows) is apparent in cytochalasin D–treated cells. (D) Number of BSA-gold–containing endosomes in EM sections. The data represent the mean ± SD (error bars). *, $P < 0.05$; **, $P < 0.005$ (unpaired *t* test comparing Ca^{2+} and Ca^{2+}/cytochalasin D samples). (E) Area occupied by vesicles containing BSA-gold in EM sections. Each symbol represents one vesicle, and the bars represent mean area ± SD. **, $P < 0.005$ (unpaired *t* test comparing Ca^{2+} and Ca^{2+}/cytochalasin D samples). (F) FACS of PI staining after scraping (NRK) or SLO (HeLa). The percentage of cells excluding PI is indicated, showing enhanced resealing in cytochalasin D–treated cells (red fill). The green dashed lines indicate the gates used to distinguish injured (PI positive) from resealed (PI negative) cell populations. Bars, 5 μm.

described (Perera et al., 2006). Before imaging, cells were treated for 20 min with 50 µg/ml cycloheximide to avoid detection of intracellular newly synthesized YFP-GPI. SLO was locally added using a microinjection system (Eppendorf). 2D compressed confocal stack images were analyzed using ImageJ software (National Institutes of Health). Kymographs were generated by uploading raw images (a time course of 2D compressed confocal stacks) into iQ software (Andor Technology), drawing a line along the periphery of a selected cell, and displaying the pixel intensity over time for each pixel along the line at each time point.

Endocytosis assays

To visualize endocytic vesicles, cells were exposed to AlexaFluor555 transferrin (Invitrogen) or SLO in Ca^{2+}/DME containing 2.5 mg/ml of lysine-fixable 10-kD Texas red (TR) dextran (Invitrogen). After 4 min at 37°C, cells were fixed, mounted in SyberGold (Invitrogen), and examined by confocal microscopy on an LSM510 microscope. Cells expressing dynamin-2 wild-type or K44A GFP constructs in pEGFP-N1 (Clontech Laboratories, Inc.) were examined by confocal microscopy for dextran or transferrin uptake 18 h after transfection (Lipofectamine). For immunofluorescence, cells were fixed in 4% PFA in DME and 10 mM Hepes/NaOH, pH 7, permeabilized in PBS, 0.05% saponin, and 1% BSA, and stained for 1 h with anti–rat Lamp1 mAb (LYIC6; provided by I. Mellman, Genentech, South San Fransisco, CA) or anti-EEA1 mAb (BD Biosciences). Nuclei were stained with DAPI (Sigma-Aldrich) or Sytox green (Invitrogen). Endocytosis was quantified by FACS after SLO or scrape wounding using a trypan blue fluorescence quench assay (Fig. S3 A; Pearson et al., 2003). Cells were stained on the plasma membrane with 1 µg/ml wheat germ agglutinin (WGA)–FITC for 1 min on ice, washed three times in PBS, wounded by scraping or by incubation with SLO, and incubated for 2 min at 37°C with 0.2% trypan blue before washing and FACS analysis.

EM

Cells treated with SLO for 4 min at 37°C or scraped from the dish and further incubated for 4 min at 37°C in Ca^{2+}/DME containing BSA-gold (OD of 520 nm = 200; Slot and Geuze, 1985) were processed for transmission EM as previously described (Rodriguez et al., 1997). Quantification was performed by counting all vesicles containing BSA-gold (including clathrin-coated vesicles, which corresponded to <7% of all vesicles found after 4 min) in 20 cell sections/sample (which contained 60–200 vesicles in the Ca^{2+} conditions). The area of all vesicles found in the sections was measured using the outline function of ImageJ.

Online supplemental material

Fig. S1 shows that Ca^{2+} is required for the repair of SLO pores and that Cherry-SLO has pore-forming activity. Fig. S2 shows that SLO-induced blebs are not responsible for plasma membrane resealing. Fig. S3 shows controls for the WGA-FITC/trypan blue endocytosis assay and EM illustrating the enlargement of lesion-induced endosomes after cytochalasin D. Video 1 shows the transient Ca^{2+} influx caused by SLO pores. Video 2 shows the rapid Ca^{2+}-dependent block in FM1-43 influx after SLO permeabilization, reflecting plasma membrane repair. Video 3 shows the rapid block in FM1-43 influx after SLO/Ca^{2+} in cells treated with cytochalasin D, a treatment that blocks blebbing. Videos 4 and 5 show that endosomes form a few seconds after SLO permeabilization. Video 6 shows that Cherry-SLO remains associated with the plasma membrane in the absence of Ca^{2+}. Video 7 shows that Cherry-SLO is internalized in the presence of Ca^{2+}. Online supplemental material is available at http://www.jcb.org/cgi/content/full/jcb.200708010/DC1.

We thank R. Tweten (University of Oklahoma, Norman, OK), W. Mothes (Yale University, New Haven, CT), and I. Mellman for plasmids and antibodies, H. Tan and R. Leone (Yale University) for help with figure and video file preparation, C. Huynh and A. Flannery for help with manuscript preparation, and R. Colvin (Massachusetts General Hospital, Boston, MA) and S. Mayor (National Center for Biological Sciences, Bangalore, India) for helpful discussions.

This work was supported by grants from the National Institutes of Health (to N.W. Andrews and C. Tam). Microscopy was supported by a National Science Foundation Major Research Instrumentation grant (to D. Toomre) and partnership with Olympus USA.

Submitted: 2 August 2007
Accepted: 5 February 2008

References

Browne, K.A., E. Blink, V.R. Sutton, C.J. Froelich, D.A. Jans, and J.A. Trapani. 1999. Cytosolic delivery of granzyme B by bacterial toxins: evidence that endosomal disruption, in addition to transmembrane pore formation, is an important function of perforin. *Mol. Cell. Biol.* 19:8604–8615.

Campbell, A.K., and B.P. Morgan. 1985. Monoclonal antibodies demonstrate protection of polymorphonuclear leukocytes against complement attack. *Nature.* 317:164–166.

Carney, D.F., C.L. Koski, and M.L. Shin. 1985. Elimination of terminal complement intermediates from the plasma membrane of nucleated cells: the rate of disappearance differs for cells carrying C5b-7 or C5b-8 or a mixture of C5b-8 with a limited number of C5b-9. *J. Immunol.* 134:1804–1809.

Charras, G.T., C.K. Hu, M. Coughlin, and T.J. Mitchison. 2006. Reassembly of contractile actin cortex in cell blebs. *J. Cell Biol.* 175:477–490.

Cocucci, E., G. Racchetti, P. Podini, M. Rupnik, and J. Meldolesi. 2004. Enlargeosome, an exocytic vesicle resistant to nonionic detergents, undergoes endocytosis via a nonacidic route. *Mol. Biol. Cell.* 15:5356–5368.

Cocucci, E., G. Racchetti, P. Podini, and J. Meldolesi. 2007. Enlargeosome traffic: exocytosis triggered by various signals is followed by endocytosis, membrane shedding or both. *Traffic.* 8:742–757.

Gmitter, D., C.O. Brostrom, and M.A. Brostrom. 1996. Translational suppression by Ca2+ ionophores: reversibility and roles of Ca2+ mobilization, Ca2+ influx, and nucleotide depletion. *Cell Biol. Toxicol.* 12:101–113.

Gundelfinger, E.D., M.M. Kessels, and B. Qualmann. 2003. Temporal and spatial coordination of exocytosis and endocytosis. *Nat. Rev. Mol. Cell Biol.* 4:127–139.

Jaiswal, J.K., G. Marlow, G. Summerill, I. Mahjneh, S. Mueller, M. Hill, K. Miyake, H. Haase, L.V. Anderson, I. Richard, et al. 2007. Patients with a non-dysferlin Miyoshi myopathy have a novel membrane repair defect. *Traffic.* 8:77–88.

Keefe, D., L. Shi, S. Feske, R. Massol, F. Navarro, T. Kirchhausen, and J. Lieberman. 2005. Perforin triggers a plasma membrane-repair response that facilitates CTL induction of apoptosis. *Immunity.* 23:249–262.

Keller, P., D. Toomre, E. Diaz, J. White, and K. Simons. 2001. Multicolour imaging of post-Golgi sorting and trafficking in live cells. *Nat. Cell Biol.* 3:140–149.

Lamaze, C., A. Dujeancourt, T. Baba, C.G. Lo, A. Benmerah, and A. Dautry-Varsat. 2001. Interleukin 2 receptors and detergent-resistant membrane domains define a clathrin-independent endocytic pathway. *Mol. Cell.* 7:661–671.

McNeil, P.L. 2002. Repairing a torn cell surface: make way, lysosomes to the rescue. *J. Cell Sci.* 115:873–879.

McNeil, P.L., S.S. Vogel, K. Miyake, and M. Terasaki. 2000. Patching plasma membrane disruptions with cytoplasmic membrane. *J. Cell Sci.* 113:1891–1902.

McNeil, P.L., K. Miyake, and S.S. Vogel. 2003. The endomembrane requirement for cell surface repair. *Proc. Natl. Acad. Sci. USA.* 100:4592–4597.

Morgan, B.P. 1989. Complement membrane attack on nucleated cells: resistance, recovery and non-lethal effects. *Biochem. J.* 264:1–14.

Morgan, B.P., and A.K. Campbell. 1985. The recovery of human polymorphonuclear leucocytes from sublytic complement attack is mediated by changes in intracellular free calcium. *Biochem. J.* 231:205–208.

Morgan, B.P., J.R. Dankert, and A.F. Esser. 1987. Recovery of human neutrophils from complement attack: removal of the membrane attack complex by endocytosis and exocytosis. *J. Immunol.* 138:246–253.

Ninomiya, Y., T. Kishimoto, Y. Miyashita, and H. Kasai. 1996. Ca2+-dependent exocytotic pathways in Chinese hamster ovary fibroblasts revealed by a caged-Ca2+ compound. *J. Biol. Chem.* 271:17751–17754.

Oh, P., D.P. McIntosh, and J.E. Schnitzer. 1998. Dynamin at the neck of caveolae mediates their budding to form transport vesicles by GTP-driven fission from the plasma membrane of endothelium. *J. Cell Biol.* 141:101–114.

Pearson, A.M., K. Baksa, M. Ramet, M. Protas, M. McKee, D. Brown, and R.A. Ezekowitz. 2003. Identification of cytoskeletal regulatory proteins required for efficient phagocytosis in *Drosophila*. *Microbes Infect.* 5:815–824.

Perera, R.M., R. Zoncu, L. Lucast, P. De Camilli, and D. Toomre. 2006. Two synaptojanin 1 isoforms are recruited to clathrin-coated pits at different stages. *Proc. Natl. Acad. Sci. USA.* 103:19332–19337.

Reddy, A., E. Caler, and N. Andrews. 2001. Plasma membrane repair is mediated by Ca2+-regulated exocytosis of lysosomes. *Cell.* 106:157–169.

Rodriguez, A., P. Webster, J. Ortego, and N.W. Andrews. 1997. Lysosomes behave as Ca2+-regulated exocytic vesicles in fibroblasts and epithelial cells. *J. Cell Biol.* 137:93–104.

Shaner, N.C., R.E. Campbell, P.A. Steinbach, B.N. Giepmans, A.E. Palmer, and R.Y. Tsien. 2004. Improved monomeric red, orange and yellow fluorescent proteins derived from *Discosoma* sp. red fluorescent protein. *Nat. Biotechnol.* 22:1567–1572.

Slot, J.W., and H.J. Geuze. 1985. A new method of preparing gold probes for multiple-labeling cytochemistry. *Eur. J. Cell Biol.* 38:87–93.

Steinhardt, R.A., B. Guoqiang, and J.M. Alderton. 1994. Cell membrane resealing by a vesicular mechanism similar to neurotransmitter release. *Science.* 263:390–393.

Togo, T., T.B. Krasieva, and R.A. Steinhardt. 2000. A decrease in membrane tension precedes successful cell-membrane repair. *Mol. Biol. Cell.* 11:4339–4346.

Tweten, R.K. 2005. Cholesterol-dependent cytolysins, a family of versatile pore-forming toxins. *Infect. Immun.* 73:6199–6209.

van der Bliek, A.M., T.E. Redelmeier, H. Damke, E.J. Tisdale, E.M. Meyerowitz, and S.L. Schmid. 1993. Mutations in human dynamin block an intermediate stage in coated vesicle formation. *J. Cell Biol.* 122:553–563.

Walev, I., S.C. Bhakdi, F. Hofmann, N. Djonder, A. Valeva, K. Aktories, and S. Bhakdi. 2001. Delivery of proteins into living cells by reversible membrane permeabilization with streptolysin-O. *Proc. Natl. Acad. Sci. USA.* 98:3185–3190.